THE JOURNAL OF PHYSICAL CHEMISTRY C

Article

Cite This: J. Phys. Chem. C 2019, 123, 3203−3215

pubs.acs.org/JPCC

Non-Kasha Behavior in Quadrupolar Dye Aggregates: The Red-Shifted H-Aggregate

Chenyu Zheng,[†,‡,§] Chuwei Zhong,[∥] Christopher J. Collison,[†,‡,§] and Frank C. Spano*[,∥]

[†]School of Chemistry and Materials Science, [‡]Nanopower Research Laboratory, and [§]Microsystems Engineering, Rochester Institute of Technology, Rochester, New York 14623, United States

[∥]Department of Chemistry, Temple University, 130 Beury Hall, 1901 N. 13th Street, Philadelphia, Pennsylvania 19122, United States

Supporting Information

ABSTRACT: Aggregates of quadrupolar DAD-type chromophores are investigated theoretically using the essential states model (ESM) enhanced to include vibronic coupling. On the basis of vibronic signatures in the absorption and photoluminescence spectra, important connections are made to the Frenkel exciton model, which is the basis for defining conventional H- and J-aggregates. In contrast to the exciton theory, the ESM allows for an unusual type of the *red-shifted* H-aggregate, driven by the large quadrupole−quadrupole interaction. Except for the red shift of the main absorption peak, such aggregates display all of the characteristics of conventional H-aggregates, including suppressed radiative decay rates and all of the vibronic signatures in the absorption and photoluminescence spectra consistent with Frenkel exciton models. Red-shifted H-dimers occur for a range of slip angles, which separate conventional H- and J-aggregate behavior, with the slip range diminishing with increasing intermolecular separation. Davydov splitting and vibronic signatures for dimers with nonparallel transition dipole moments are also investigated. The theoretical insight provided herein may be exploited for optimizing optoelectronic device applications for growing families of quadrupolar molecules.

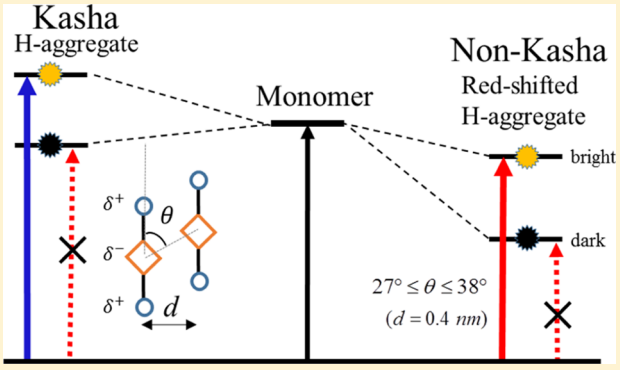

1. INTRODUCTION

Quadrupolar conjugated molecules are increasingly investigated for application in optoelectronic devices because of the feasibility of energy level engineering and strong charge delocalization properties.[1,2] For example, squaraines (SQs) are typical near-infrared-absorbing quadrupolar molecules, which have been used successfully as absorbers in organic photovoltaic (OPV) devices,[3−7] as well as two-photon absorption sensors and fluorescent probes.[8−10] SQs represent a larger class of push−pull molecules where a critical strategy for OPV design is to tailor highest occupied molecular orbital and lowest unoccupied molecular orbital energy levels based on the relative strengths of intramolecular electron-donating or -accepting groups.[11,12]

SQs and quadrupolar aggregates in general also have a significant value in that they allow some assessment of the impact of aggregation on the excitonic diffusion length and charge mobility in OPV devices.[5,13,14] We focus here on the NIR-vis spectral response of these aggregates, which contains valuable clues about the nature of the underlying excitons. Indeed, we show how quadrupolar dye aggregates can display highly unconventional (non-Kasha) spectroscopic behavior. Only when a full understanding of the photophysics is achieved, can we most effectively design the molecular structure for optimal performance in device applications.

The Kasha model is usually the starting point for describing spectroscopic phenomena in molecular aggregates.[15−17] The model is based on Frenkel exciton theory in which two-level chromophores are coupled via dipole−dipole interactions, most often under the point dipole approximation. Aggregates of pseudoisocyanine molecules are the classic examples of the so-called J-aggregates in which molecules arrange in a head-to-tail fashion, resulting in a negative Coulomb coupling and consequently the deposition of oscillator strength in the lowest-energy exciton.[18−20] This is manifest photophysically as a narrow red-shifted absorption band relative to the unaggregated (monomer) in solution and a radiative decay rate which scales with the number of molecules in the aggregate. Conversely, in H-aggregates, which result from side-to-side packing, the positive sign for Coulomb coupling and the resulting deposition of oscillator strength in the highest-energy exciton lead to a generally blue-shifted absorption spectrum and a suppressed radiative decay rate.

Received: November 26, 2018
Revised: December 26, 2018
Published: January 28, 2019

Downloaded via TU GRAZ on January 5, 2023 at 18:27:25 (UTC).
See https://pubs.acs.org/sharingguidelines for options on how to legitimately share published articles.

ACS Publications © 2019 American Chemical Society

DOI: 10.1021/acs.jpcc.8b11416
J. Phys. Chem. C 2019, 123, 3203−3215

One of the shortcomings of Kasha's approach is that the underlying Frenkel exciton model, which is based on a two-level (S_0 and S_1) molecular chromophore, does not directly account for polarizability effects such as the gas-to-crystal shift. The latter is dominated by nonresonant intermolecular interactions between S_0 and S_1 and the multitude of higher excited states not included in the Hamiltonian, the overall effect of which (usually) is an enhanced stabilization of the excited state relative to the ground state, as manifest by a spectral red shift in the absorption spectrum. Normally, the gas-to-crystal shift is incorporated as an empirical parameter, which corrects the on-site (molecular) transition energy in the Frenkel Hamiltonian. For molecules with low polarizabilities, such as the perylenes[21] and oligoacenes,[22] the Kasha/Frenkel model provides an excellent description of the aggregate photophysics. However, for donor−acceptor molecules (DA, DAD, ...), the $S_0 \rightarrow S_1$ transition involves significant charge redistribution, which results in very large polarizabilities. Aggregates of such molecules exhibit a photophysical behavior not generally accounted for by the Kasha theory, as underscored by Painelli and co-workers who pioneered the essential states model (ESM)[23−26] in order to more accurately capture polarizability effects. In the ESM, each molecule is described in a basis of diabatic states which differ from each other by significant charge displacement. The coupling between such diabatic states results in the molecular ground and excited states (i.e., S_0 and S_1), which, unlike in the exciton model, are "fluid" in the sense that their construction (in terms of the diabatic states) readily responds to local electric fields derived from intermolecular interactions or from a polar solvent environment. The ESM can therefore also account for solvatochromism and solvent-dependent changes in the vibronic peak intensities in dipolar (DA) and quadrupolar dyes.[24,25]

Marked divergences between the ESM and exciton models in describing aggregate photophysics have been identified by Sanyal et al.[26] Using the ESM, they showed the existence of a red-shifted H-aggregate for quadrupolar (DAD) dye aggregates where *both* the bright and dark excited states in a dimer aggregate are red-shifted below the monomeric transition energy. Their work was motivated by the observation of so-called "nonfluorescent J-aggregates" consisting of a water-soluble cationic SQ dye by Belfield and coworkers.[27] We should point out that red-shifted H-aggregates are not unprecedented and also arise in the Frenkel exciton model whenever the aforementioned gas-to-crystal red shift exceeds the blue shift derived from resonant dipole−dipole coupling, as is the case in some carotenoid aggregates.[28] The well-known polymer poly(3-hexylthiophene) also forms H-aggregates which are red-shifted from the unaggregated polymer in solution mainly because of chain planarization which accompanies aggregation.[29] When intermolecular charge transfer is included in the Frenkel exciton model, one can also form red-shifted H-aggregates because of short-range superexchange interactions.[30,31] The quadrupolar aggregates, however, are unique, in that the red shift of both bright and dark states derives from strong quadrupole−quadrupole interactions which exist within symmetric DAD dyes.

In this work, we extend the ESM to include vibronic coupling in symmetric DAD aggregates and revisit the red-shifted H-aggregate of Sanyal et al.[26] Particular emphasis is placed on the phase space which defines this unusual aggregate type as well as the vibronic structure originating from the main vinyl-stretching mode, expressed as progressions in the absorption and emission spectra. We are particularly interested in whether the vibronic signatures derived from the Frenkel/Holstein model for J- and H-aggregation[30−33] remain valid in the ESM. Notably, the ratio A_1/A_2 of the oscillator strengths of the first two vibronic peaks in the absorption spectrum increases (decreases) with exciton bandwidth in J-aggregates (H-aggregates), whereas the 0−0 peak in the photoluminescence (PL) spectrum is dominant in J-aggregates but is entirely absent in ideal H-aggregates (with no disorder and at low temperature).[32] Moreover, the 0−0/0−1 vibronic ratio in the PL spectrum of J-aggregates is a direct probe of N_{coh}, the number of the molecules over which the exciton is coherent.[30,33] In what follows, we limit our attention to the usual dimer slip-stacked aggregates and also consider dimer herringbone (HB) aggregates, which display Davydov splitting, a phenomenon known to arise in SQ complexes.[26,34−37]

2. MODEL

In this section, we introduce the Hamiltonian for a coupled pair of symmetric quadrupolar chromophores based on Painelli's ESM.[23−26] For quadrupolar dyes with linear D−π−A−π−D or A−π−D−π−A structures, the ESM identifies three essential states including one neutral state and two degenerate zwitterionic states, that is, D−A−D ($|N\rangle$), D^+-A^-−D ($|Z_1\rangle$), and D−A^-−D^+ ($|Z_2\rangle$), with similar definitions for A−π−D−π−A molecules. The states are depicted in Figure 1. The

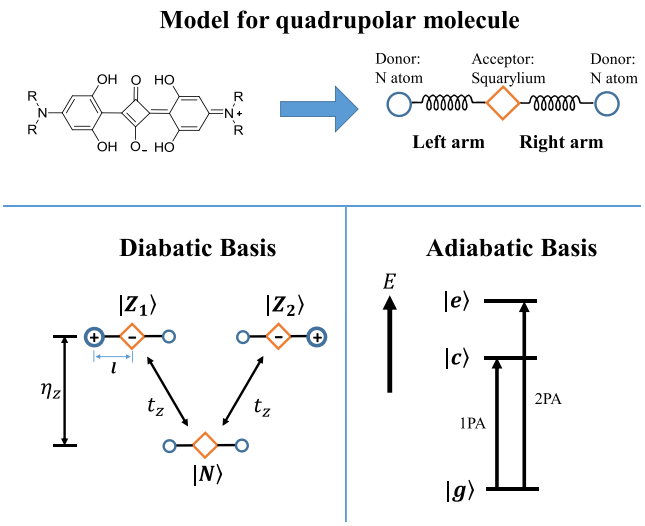

Figure 1. Illustrations of a quadrupolar dye as a three-level (D−A−D) construct in the ESM. The left and right arms bridging the donors (nitrogen atoms) and the acceptor (squarylium) can host normal vibrational modes (vinyl stretching or ring breathing). The diabatic states consist of the neutral state, $|N\rangle$, and the two charge-transfer states, $|Z_1\rangle$ and $|Z_2\rangle$. The adiabatic states, which are the eigenstates of the electronic Hamiltonian, are responsible for the optical transitions. For a linear quadrupolar chromophore, the first excited state $|c\rangle$ is one-photon allowed (1PA) and the second excited state $|e\rangle$ is two-photon allowed (2PA).

two zwitterionic states are assumed to lie above the neutral state with energy η_Z ($\eta_Z > 0$) and are coupled to the neutral state via a charge-transfer integral, t_Z. The electronic Hamiltonian for a single chromophore is therefore given as

DOI: 10.1021/acs.jpcc.8b11416
J. Phys. Chem. C 2019, 123, 3203−3215

$$\hat{H}_{\mathrm{mon}}^{\mathrm{el}} = \eta_z \sum_{a=1,2} |\mathrm{Z}_a\rangle\langle \mathrm{Z}_a| - t_z \sum_{a=1,2} \{|\mathrm{N}\rangle\langle \mathrm{Z}_a| + h.\,c.\,\} \tag{1}$$

Diagonalizing the Hamiltonian yields three "adiabatic" states, each a linear combination of the essential "diabatic" states

$$|\mathrm{g}\rangle = \sqrt{1-\rho}\,|\mathrm{N}\rangle + \sqrt{\rho/2}\,(|\mathrm{Z}_1\rangle + |\mathrm{Z}_2\rangle) \tag{2a}$$

$$|\mathrm{c}\rangle = \sqrt{1/2}\,(|\mathrm{Z}_1\rangle - |\mathrm{Z}_2\rangle) \tag{2b}$$

$$|\mathrm{e}\rangle = \sqrt{\rho}\,|\mathrm{N}\rangle - \sqrt{(1-\rho)/2}\,(|\mathrm{Z}_1\rangle + |\mathrm{Z}_2\rangle) \tag{2c}$$

where $|\mathrm{g}\rangle$ is the ground state and $|\mathrm{c}\rangle$ and $|\mathrm{e}\rangle$ are the first (one-photon allowed) and second (two-photon allowed) excited states. Here, the quantity, ρ, defined as

$$\rho = 0.5(1 - \eta_Z/\sqrt{\eta_Z^{\,2} + 8t_Z^{\,2}})$$

represents the admixture of the zwitterionic component in the molecular ground state $|\mathrm{g}\rangle$.

The energies of the adiabatic electronic states are given by

$$E_{\mathrm{g}} = \frac{1}{2}(\eta_Z - \sqrt{\eta_Z^{\,2} + 8t_Z^{\,2}}) \tag{3a}$$

$$E_{\mathrm{c}} = \eta_Z \tag{3b}$$

$$E_{\mathrm{e}} = \frac{1}{2}(\eta_Z + \sqrt{\eta_Z^{\,2} + 8t_Z^{\,2}}) \tag{3c}$$

Importantly, in both symmetry-adapted states, $\sqrt{\frac{1}{2}}(|\mathrm{Z}_1\rangle + |\mathrm{Z}_2\rangle)$ and $\sqrt{\frac{1}{2}}(|\mathrm{Z}_1\rangle - |\mathrm{Z}_2\rangle)$, positive charges $(+e/2)$ reside at the nitrogen atom centers, whereas a negative charge $(-e)$ resides at the squarylium center. The charge distribution results in a quadrupole moment (Q_{xx}) equal to ρel^2, el^2, and $(1-\rho)el^2$ in the states $|\mathrm{g}\rangle$, $|\mathrm{c}\rangle$, and $|\mathrm{e}\rangle$, respectively, where l is the arm length indicated in Figure 1. Note that the permanent dipole moment in each state is zero (unless the symmetry is broken[25]), whereas the *transition* dipole moment (TDM) between $|\mathrm{g}\rangle$ and $|\mathrm{c}\rangle$ is $\sqrt{\rho}\,el$.[25] The latter is responsible for one-photon absorption.

In order to account for molecular vibrations, one vibrational coordinate is introduced for each charge-transfer degree of freedom, thereby accounting for the nuclear geometric rearrangement resulting from charge redistribution (see Figure 1). For example, the creation of a zwitterion on the "right" arm (i.e., $\mathrm{D{-}A^{-}{-}D^{+}}$) will induce a change in the equilibrium length of that arm. In the simplest approximation, the corresponding nuclear potentials of the neutral and zwitterion arm are shifted harmonic potentials, with the shift indicating the change in equilibrium value of the most strongly coupled vibrational coordinate. Thus, the complete monomer Hamiltonian including both electronic and vibrational degrees of freedom resembles a Holstein Hamiltonian

$$\hat{H}_{\mathrm{mon}} = \hat{H}_{\mathrm{mon}}^{\mathrm{el}} + \hbar\omega_{\mathrm{vib}} \sum_{a=1,2} b_a^{\dagger} b_a + \hbar\omega_{\mathrm{vib}}\lambda_{\mathrm{dia}} \sum_{a=1,2} (b_a^{\dagger} + b_a + \lambda_{\mathrm{dia}})|\mathrm{Z}_a\rangle\langle \mathrm{Z}_a| \tag{4}$$

where $b_a^{\dagger}(b_a)$ creates (annihilates) a vibrational quantum on each molecular arm ($a = 1$, "left" arm; $a = 2$, "right" arm, see Figure 1) of the chromophore with an energy of $\hbar\omega_{\mathrm{vib}}$. The vibrational energy lies in the range 0.15−0,18 eV for the ubiquitous vinyl stretching mode characterizing most π-conjugated molecules. The local vibronic coupling is reflected in the third term of eq 4, where the nuclear potential energy surface of the zwitterionic state is taken to be displaced by λ_{dia} as compared to the neutral state. The quantity, $\lambda_{\mathrm{dia}}^{\,2}$, is the diabatic Huang−Rhys (HR) factor.

In aggregates of quadrupolar chromophores, the molecules interact with each other Coulombically, as in the Kasha exciton model.[15−17] For a dimer, the Hamiltonian reads

$$\hat{H}_{\mathrm{dimer}} = \sum_{n=1}^{2} \hat{H}_{\mathrm{n}}^{\mathrm{mon}} + \frac{1}{4\pi\varepsilon\varepsilon_0} \sum_{a,b} \sum_{i,j} \frac{q_1(a,i)q_2(b,j)}{|\boldsymbol{r}_1(a,i) - \boldsymbol{r}_2(b,j)|} |\mathrm{Z}_a\mathrm{Z}_b\rangle\langle \mathrm{Z}_a\mathrm{Z}_b| \tag{5}$$

where the dimer basis function $|\mathrm{Z_aZ_b}\rangle$ indicates the electronic states of the two chromophores. The Coulombic coupling term in eq 5 is calculated in the diabatic basis with the charge densities collapsed to the centers of the donor or acceptor molecular sites, with the Coulombic interactions restricted to charges located on different molecules. The charge distribution which corresponds to the Z_a zwitterion (a = 1,2) on the chromophore n is denoted as $q_n(a,i)$, where i = 1, 2, or 3 indicates the "left" donor, central acceptor, and "right" donor respective charge centers, as indicated in Figure 1. Hence, for the zwitterion Z_1, we have $q_n(1,i=1) = +e$, $q_n(1,i=2) = -e$, and $q_n(1,i=3) = 0$ for the nth chromophore. Finally, $\boldsymbol{r}_n(a,i)$ is the position vector for the corresponding point charge, which is defined by the dimer geometry and the arm length, l. ε and ε_0 are the (relative) dielectric constant and vacuum permittivity, respectively. Here, ε accounts for screening effects derived from electronic excited states beyond the essential states. A detailed description of the electronic/vibrational basis set used to represent the Hamiltonian in eq 5 can be found in the Supporting Information.

3. VIBRONIC COUPLING IN A MONOMER

In contrast to the ESM, in the vibronic exciton theory, a chromophore consists of just two electronic levels with the ground- and excited-state nuclear potentials represented by shifted harmonic wells.[32] In such a monomer, the optical absorption spectrum takes the form of a vibronic progression with peak frequencies occurring at $\omega_{0-\nu} = \omega_{0-0} + \nu\omega_{\mathrm{vib}}$, where ν = 0, 1, 2, ... indicates the number of vibrational quanta in the excited-state potential. The $0-\nu$ peak intensities are governed primarily by the Franck−Condon (FC) factors

$$f^{0-\nu} = \mathrm{e}^{-\lambda^2}\frac{\lambda^{2\nu}}{\nu!} \qquad \nu = 0, 1, 2, \tag{6}$$

where λ^2 is the HR factor which accounts for the relative displacement of the ground and excited harmonic wells. We note that in addition to the FC factor, the oscillator strength of the $0-\nu$ peak also contains the transition energy, $\omega_{0-\nu}$, which only slightly affects the relative peak intensities when the vibrational energy is much less than the optical transition energy ($\omega_{\mathrm{vib}} \ll \omega_{0-0}$), as is usually the case.

A monomer in the ESM is considerably more complex than the simple two-level chromophore just described.[23−26] The harmonic wells corresponding to the two vibrational modes (one for each arm) correspond to the diabatic or "premixed" essential electronic states, with the HR factor for each mode

DOI: 10.1021/acs.jpcc.8b11416
J. Phys. Chem. C 2019, 123, 3203−3215

given by λ_{dia}^2. Only after diagonalizing the monomer Hamiltonian to obtain the adiabatic states can one establish the validity of an effective adiabatic HR factor, which describes the relative shift of the adiabatic ground- and excited-state harmonic wells. This is possible when the conditions, t_Z, $\eta_Z \gg \hbar\omega_{vib}$ and $t_z \gtrsim \eta_Z$, are satisfied, allowing the vibronic coupling to be treated perturbatively (see Supporting Information Section II for details). The resulting effective *adiabatic* HR factor is

$$\lambda^2 = \frac{(1-\rho)^2}{2}\lambda_{dia}^2 \tag{7}$$

which corresponds to the relative shift of the harmonic wells of the ground state, |g⟩, and (one-photon allowed) excited state, |c⟩. Equation 7 shows that the vibronic structure in the linear absorption and fluorescence spectra of quadrupolar dyes depends on both the diabatic HR factor and the quantity, ρ, introduced in Section 2. For typical class I/II quadrupolar chromophores[25] considered in this work, the value of ρ lies in the range, $0 < \rho < 0.5$. According to eq 7, when $\rho \approx 0.5$, a value appropriate for SQ dyes, λ^2 is only 1/8 of λ_{dia}^2. As the value $\lambda_{dia}^2 = 1$ is typically used to describe the vinyl stretching mode in SQ dyes,[23−25] the ratio f^{0-0}/f^{0-1} is about 8, indicating a dominant 0−0 peak in the vibronic progression of the absorption spectrum. Indeed, the side-band 0−1 transition for many SQ dyes is observed to be far weaker than the origin (0−0).[38−40]

To demonstrate the validity of eq 7, the monomer absorption spectrum of a SQ dye was calculated using $\lambda_{dia}^2 = 1$ and $\lambda_{dia}^2 = 3$, with the latter value chosen to emphasize the vibronic progression. The results are shown in Figure 2. The

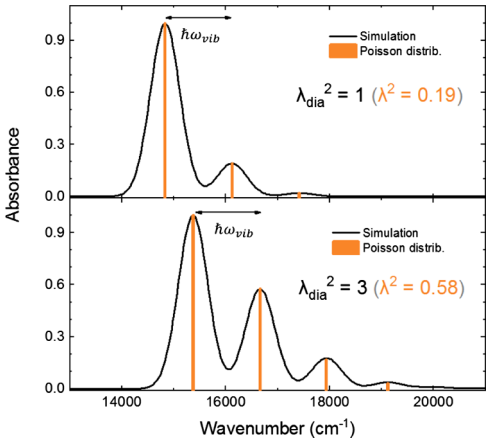

Figure 2. Calculated absorption spectrum based on eq S12 for quadrupolar chromophores with $\lambda_{dia}^2 = 1$ (top) and $\lambda_{dia}^2 = 3$ (bottom) for a vibrational mode with $\hbar\omega_{vib} = 0.16$ eV. The electronic parameters are selected based on a SQ chromophore: $\eta_Z = 0.7$ eV, $t_Z = 1.0$ eV, which gives $\rho = 0.38$. The vibronic peak intensities correspond well with the Poisson distribution (eq 6) indicated by the bars with the adiabatic HR factor, λ^2, obtained from eq 7.

ESM parameters listed in the figure caption correspond to typical SQ quadrupolar dyes.[25,41] The spectra demonstrate that the ratio of the first two vibronic peak intensities, $\approx f^{0-0}/f^{0-1}$, is well accounted for by $1/\lambda^2$, where λ^2 is obtained from eq 7 and given in the figure insets. In fact, the entire progression is well described by eq 6 using the effective HR factor λ^2, as demonstrated by the bars in each spectrum.

We have simulated the absorption spectra for a range of quadrupolar dyes with different values of ρ, selecting η_Z to be in the 1−3 eV range, which covers most quadrupolar dyes,[25,26,41,42] and varying t_Z from zero to $2\eta_Z$. The calculated values of $\lambda^2/\lambda_{dia}^2$ are shown in Figure 3, which also includes the

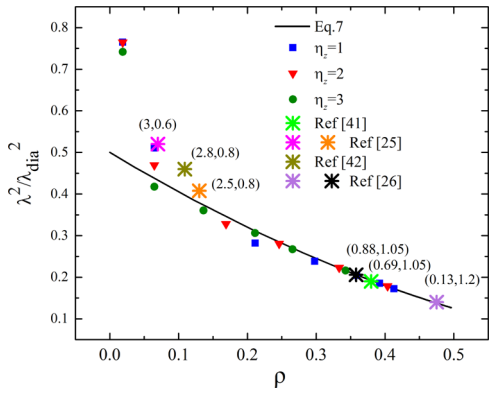

Figure 3. $\lambda^2/\lambda_{dia}^2$ as a function of ρ for quadrupolar chromophores. The solid black curve represents $\lambda^2/\lambda_{dia}^2$ obtained from eq 7. For selected points, λ^2, is obtained from the 0−0 and 0−1 intensity ratios in simulations where η_Z is set to 1, 2, and 3 eV, while the coupling t_Z is varied within the interval, $0 < t_Z < 2\eta_Z$ (causing ρ to vary from 0 to 0.41). In all cases, the vibrational parameters are $\hbar\omega_{vib} = 0.16$ eV and $\lambda_{dia}^2 = 1$. In addition, six points corresponding to published parameter sets used for comparisons to experiments are shown (asterisks), with the (η_Z, t_Z) values in electronvolt indicated above each point. The black line agrees well with the numerical simulations when $\rho > 0.1$ because for small values of ρ, the perturbation condition ($\hbar\omega_{vib} \ll t_Z\eta_Z$) breaks down.

values for six quadrupolar dyes, which have been simulated previously to compare with experiments.[25,41,42] The simulation data points basically fall on the line calculated from eq 7, except for a few points having $\rho < 0.1$. Such exceptions arise because for small ρ values, t_Z is much smaller than η_Z and likely also much smaller than the vibrational energy, $\hbar\omega_{vib}$, which invalidates the perturbation assumption.

Grisanti et al. have derived a similar expression to eq 7 but for a DA molecule hosting just two essential (diabatic) states[24]

$$\lambda^2 = (1-2\rho)^2\lambda_{dia}^2$$

The lack of a factor 2 in front of ρ in eq 7 is related to the additional zwitterionic states of the quadrupole, whereas the presence of a factor 2 in the denominator in eq 7 indicates a reduction in vibronic coupling because of enhanced delocalization. This is qualitatively consistent with the general observation for polymers that the effective HR factor is a decreasing function of chain length.[43]

4. DIMER AGGREGATES OF QUADRUPOLAR DYES

In this section, we consider the impact of intermolecular Coulombic interactions in eq 5 on the structure of the eigenstates in dimer aggregates of quadrupolar dyes under the ESM. In the Kasha exciton model, the Coulomb coupling induces a splitting of the local degenerate excited states into an upper and a lower exciton state with respect to the monomer transition energy. For aggregates with aligned molecular TDMs, H-aggregates (J-aggregates) are formed when the coupling is positive (negative), resulting in the placement of the "bright" state at the top (bottom) of the band, leading to previously mentioned blue- (red-) shifted absorption peaks.

DOI: 10.1021/acs.jpcc.8b11416
J. Phys. Chem. C 2019, 123, 3203−3215

Similarly, the categorization of J- and H-aggregates in the ESM also depends on the ordering of the bright and dark states induced by intermolecular interactions, but the relationship to spectral shifts is not as clear as in the Kasha model because of the highly polarizable chromophores. As Painelli et al. have pointed out, there exists a unique phase where both bright and dark states shift downward compared to the monomer excited state, leading to a red-shifted H-aggregate, which has also been referred to as a "nonfluorescent" J-aggregate.[27]

To understand the impact of Coulomb coupling on the dimer excited states, we first consider the simpler case *without* vibronic coupling. Expressing the dimer diabatic states as direct products of monomer states gives a total of nine states: $|NN\rangle$, $|NZ_1\rangle$, $|NZ_2\rangle$, $|Z_1N\rangle$, $|Z_2N\rangle$, $|Z_1Z_1\rangle$, $|Z_1Z_2\rangle$, $|Z_2Z_1\rangle$, $|Z_2Z_2\rangle$, where the first (second) entry indicates the state of the first (second) chromophore. In this basis set, the Coulombic energy is diagonal, with the states $|Z_1Z_1\rangle$, $|Z_1Z_2\rangle$, $|Z_2Z_1\rangle$, and $|Z_2Z_2\rangle$ possessing the energies, V_{11}, V_{12}, V_{21}, and V_{22}, respectively. In order to understand how the Coulomb coupling impacts excited states, the Coulombic terms were treated perturbatively. Thus, the Hamiltonian is divided into an unperturbed term

$$\begin{aligned}\hat{H}^0 = {} & \eta_z \sum_{a=1,2} (|NZ_a\rangle\langle NZ_a| + |Z_aN\rangle\langle Z_aN|) \\ & + 2\eta_z \sum_{a,b} |Z_aZ_b\rangle\langle Z_aZ_b| \\ & - t_z \sum_{a} \{|NN\rangle\langle NZ_a| + |NN\rangle\langle Z_aN| + h.\,c.\,\} \\ & - t_z \sum_{a,b} \{|Z_aZ_b\rangle\langle NZ_b| + |Z_aZ_b\rangle\langle Z_aN| + h.\,c.\,\}\end{aligned} \tag{8a}$$

and the Coulombic perturbation term

$$\hat{H}' = \sum_{a,b} V_{ab} |Z_aZ_b\rangle\langle Z_aZ_b| \tag{8b}$$

In what follows, we consider two dimer geometries: a slip-stack (SS) dimer with aligned molecular TDMs and a HB dimer with an oblique TDM alignment as depicted in Figure 4. As in the exciton model, two excited states arise, only one of which is one-photon allowed in the SS geometry, whereas both are allowed, but orthogonally polarized, in the HB geometry, giving rise to a Davydov splitting. To zero-order, the excited states are denoted as $|gc\rangle^S$ and $|gc\rangle^{AS}$, which are eigenstates of the Hamiltonian in eq 8aa. (Here, g and c indicate the ground and one-photon allowed monomer states, see eq 2a). The two excited states have opposing symmetries: for the SS geometry, $|gc\rangle^S$ and $|gc\rangle^{AS}$ are, in turn, symmetric and antisymmetric with respect to the inversion center, and in the HB aggregate, the corresponding symmetry element is a C_2 rotation axis, which bisects the angle formed by the two chromophores (see Figure 4). To zeroth order, the symmetry-adapted states take the forms

$$|gc\rangle^S = \frac{1}{\sqrt{2}}(|gc\rangle + |cg\rangle) \tag{9a}$$

and

$$|gc\rangle^{AS} = \frac{1}{\sqrt{2}}(|gc\rangle - |cg\rangle) \tag{9b}$$

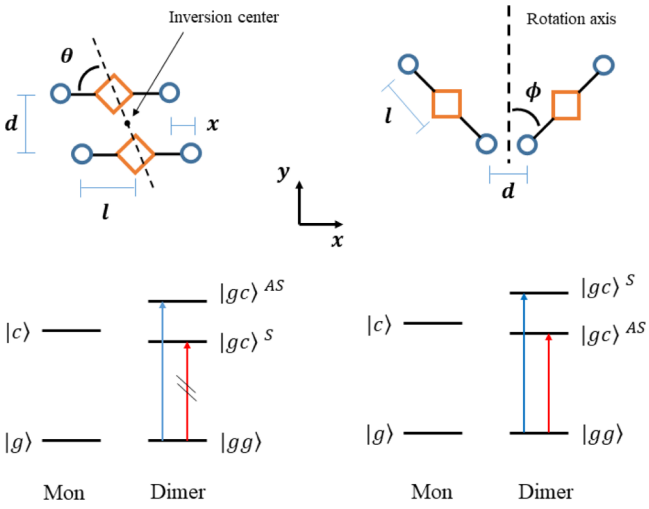

Figure 4. SS (left) and HB structures (right) for the quadrupole dimers investigated in this work. The allowed and forbidden transitions between electronic states are shown in the bottom for each packing structure. The symmetry of the excited states is defined using an inversion center for the SS dimer and by using a twofold rotation for the HB dimer. For the SS dimer, the antisymmetric bright state lies higher (lower) in energy than the symmetric dark state in H- (J-) aggregates. For the HB dimer, both states absorb light.

Here, as in ref 41, we define the phase of the wave function on chromophore 2 relative to chromophore 1 using the appropriate symmetry operation. For example, in the SS geometry, $|cg\rangle = \hat{i}|gc\rangle$, where $\hat{i}$ is the inversion operator. In the diabatic basis, this is consistent with the state, $|Z_1 - Z_2\rangle$ on chromophore "1" becoming $|Z_2 - Z_1\rangle$, on chromophore "2" upon inversion, as can be appreciated from Figure 4.

For the linear (one-photon allowed) absorption and emission spectra, we need to only consider the ground state, $|gg\rangle$, and the two low-lying excited states. Higher-energy eigenstates are also obtained from the dimer Hamiltonian but are not relevant to the linear absorption study. In terms of the diabatic states, the symmetry-adapted dimer states for the SS dimer correct to zeroth-order are written as

$$\begin{aligned}|gg\rangle = {} & (1-\rho)|NN\rangle + \sqrt{\rho(1-\rho)}\,(|NZ_+\rangle + |Z_+N\rangle) \\ & + \rho|Z_+Z_+\rangle\end{aligned} \tag{10a}$$

$$\begin{aligned}|gc\rangle^S = {} & \sqrt{\frac{1-\rho}{2}}\,(|NZ_-\rangle - |Z_-N\rangle) \\ & + \sqrt{\frac{\rho}{2}}\,(|Z_+Z_-\rangle - |Z_-Z_+\rangle)\end{aligned} \tag{10b}$$

$$\begin{aligned}|gc\rangle^{AS} = {} & \sqrt{\frac{1-\rho}{2}}\,(|NZ_-\rangle + |Z_-N\rangle) \\ & + \sqrt{\frac{\rho}{2}}\,(|Z_+Z_-\rangle + |Z_-Z_+\rangle)\end{aligned} \tag{10c}$$

where we have introduced the symmetry-adapted diabatic states $|Z_+\rangle \equiv 2^{-1/2}\{|Z_1\rangle + |Z_2\rangle\}$ and $|Z_-\rangle \equiv 2^{-1/2}\{|Z_1\rangle - |Z_2\rangle\}$. For the HB geometry, the symmetric and antisymmetric excited states are reversed and are given by eq 10c and eq 10b, respectively. This is because under C_2 rotation $|Z_-\rangle$ on chromophore 1 becomes $|Z_-\rangle$ on chromophore 2, and not $-|Z_-\rangle$ as happens under inversion.

DOI: 10.1021/acs.jpcc.8b11416
J. Phys. Chem. C 2019, 123, 3203−3215

To zero-order, the energy difference between $|gc\rangle^S$ (or $|gc\rangle^{AS}$) and the ground state, $|gg\rangle$, is identical to the monomer's transition energy, as the molecules in the dimer have yet to Coulombically interact with each other. In what follows, we will evaluate the state energies to first order in the Coulomb interaction for both dimer geometries, making additional connections to the exciton theory.

4.1. SS dimer. Note that because the TDM operator is antisymmetric with respect to inversion in the SS geometry, the state $|gc\rangle^{AS}$ is optically allowed from the ground state, whereas $|gc\rangle^S$ is optically forbidden. Hence, we have

$$\langle gg|\hat{\mu}|gc\rangle^S = 0 \tag{11a}$$

and

$$\langle gg|\hat{\mu}|gc\rangle^{AS} = el\sqrt{2\rho} \tag{11b}$$

Here, $\hat{\mu}$ is the dipole moment operator as expressed in eq S11b and $el\sqrt{\rho}$ is the molecular TDM, with l the length between the negative and positive charge centers (see Figure 1 or 4). Hence, $|gc\rangle^S$ is "dark" because of a cancellation of molecular TDMs on each chromophore, whereas $|gc\rangle^{AS}$ is "bright" with an enhanced oscillator strength relative to the monomer because of an in-phase arrangement of transition dipoles. This assignment is analogous to the two Frenkel excited states in Kasha's exciton model. Hence, the ordering of the states $|gc\rangle^S$ and $|gc\rangle^{AS}$ with respect to energy should serve to unambiguously identify J- and H-aggregates in the ESM; when the optically allowed $|gc\rangle^{AS}$ state is located above (below) the dark $|gc\rangle^S$ state, an H- (J-) aggregate, defined through its photophysical properties, including spectral shifts, fluorescence yields, and vibronic signatures, should result.

The Coulomb perturbation $\hat{H}'$ lifts the degeneracy of the symmetric and antisymmetric excited states. The first-order energy corrections for $|gc\rangle^S$ and $|gc\rangle^{AS}$ states are given by

$$E^{(1)}_{|gc\rangle^S} = {}^S\langle gc|\hat{H}'|gc\rangle^S = \frac{\rho}{2}(V_{12} + V_{21}) \tag{12a}$$

$$E^{(1)}_{|gc\rangle^{AS}} = {}^{AS}\langle gc|\hat{H}'|gc\rangle^{AS} = \frac{\rho}{2}(V_{11} + V_{22}) \tag{12b}$$

Thus, the order of excited states depends on the four Coulombic terms, V_{ij}. Note that ρ is a common factor in both eqs 12a and 12b so that the splitting of the two states scales linearly with the zwitterionic admixture. As shown later on, the first-order corrections reduce to familiar point dipole−dipole expressions for large intermolecular separations.

Another important consequence of the Coulombic coupling is the ground-state energy correction, which is driven by the quadrupole−quadrupole interaction

$$E^{(1)}_{|gg\rangle} = \langle gg|\hat{V}|gg\rangle = \frac{\rho^2}{4}(V_{11} + V_{12} + V_{21} + V_{22}) \tag{12c}$$

As a result, the transition energy from $|gg\rangle$ to the optically allowed state, $|gc\rangle^{AS}$, complicates the classification of H- or J-aggregation based on spectral shifts alone. Although the J/H definition depends on the ordering of the symmetric and antisymmetric excited states, it may not be generally true that J-aggregates and H-aggregates are respectively red-shifted and blue-shifted away from the monomer energy. One needs to be careful in assigning J- and H-aggregation based solely on spectral shifts.

To better appreciate possible unconventional behavior posed by the SS SQ dimers, we investigate the energetic ordering of the states as well as the aggregate transition energy relative to that of the monomer, as a function of the molecular "slip" distance, Δx, and the intermolecular separation, d (see Figure 4). We define the slip angle θ as $\tan\theta = d/\Delta x$, such that $\Delta x = 0$ corresponds to $\theta = 90°$, that is, the two chromophores are "side-by-side" as indicated in Figure 4. For typical SQ dyes, the "arm length" is $l \approx 6$ Å,[25,26] whereas d is ∼4 Å in packing geometries based on π-stacking. Using these values, the first-order energy shifts of the ground and both excited states as a function of slip angle θ are computed using eqs 12a−12c and shown in Figure 5.

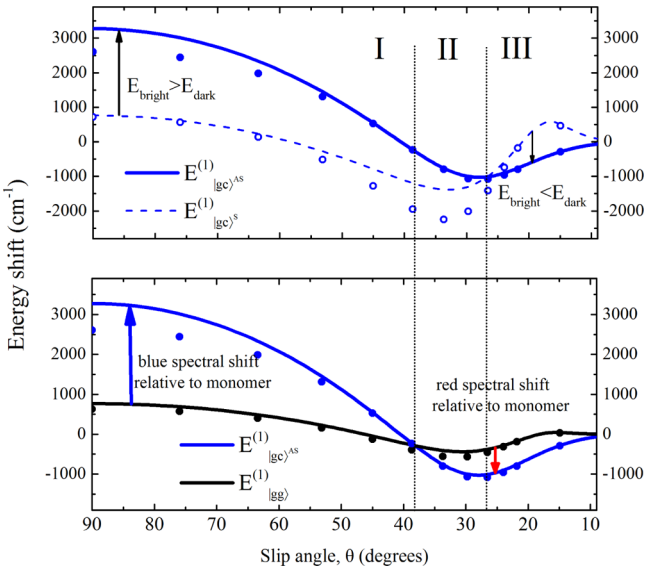

Figure 5. (Top) First-order energy correction for the antisymmetric bright state $|gc\rangle^{AS}$ (solid blue line) and the symmetric dark state $|gc\rangle^S$ (dashed blue line) as a function of slip angle, θ, based on eqs 12a−12c. The exact numerically evaluated energies based on the Hamiltonian in eq 5 (but without vibronic coupling) are shown as filled (bright state) and hollow (dark state) dots. (Bottom) First-order energy correction to the ground-state $|gg\rangle$ energy (solid black curve) alongside the exact energies (solid black dots). The first-order correction to the bright state is replotted. In all calculations, the structural parameters are taken to be $l = 6$ Å and $d = 4$ Å, whereas the monomer electronic parameters, $\eta = 0.7$ eV and $t_Z = 1$ eV ($\rho = 0.38$), are consistent with a typical SQ monomer (see ref 41). In addition, the coupling strength is screened by a dielectric constant of 3. The two vertical dashed lines demarcate three phases, I, II, and III (see the text for details). At $\theta = 38.1°$ (indicated by the first vertical line), the aggregate-induced spectral shift reverses sign, whereas at $\theta = 26.9°$ (indicated by the second vertical line), the bright and dark state energies reverse their order. Note that the phase boundaries are essentially the same using either exact or first-order energies.

On the basis of the energetic ordering of the bright and dark states in the dimer as well as the spectral shift of the dimer relative to the monomer, we identify three phase regions in Figure 5. In phase I, defined by slip angles in the range, $38.1° \leq \theta \leq 90°$, the optically bright state, $|gc\rangle^{AS}$, lies above the dark state, $|gc\rangle^S$ ($E^{(1)}_{|gc\rangle^{AS}} > E^{(1)}_{|gc\rangle^S}$) and the dimer experiences a blue spectral shift relative to the monomer ($E^{(1)}_{|gc\rangle^{AS}} > E^{(1)}_{|gg\rangle}$). In addition, the fluorescence is suppressed because the lowest-energy state is dark. Hence, in this region, the dimer exhibits a typical H-aggregate behavior as originally described by Kasha.

DOI: 10.1021/acs.jpcc.8b11416
J. Phys. Chem. C 2019, 123, 3203−3215

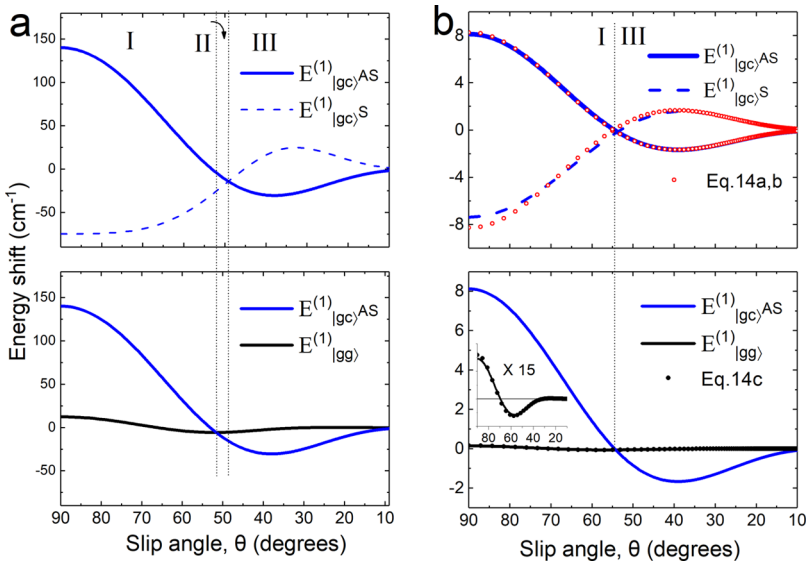

Figure 6. First-order energy corrections in eqs 12a−12c as a function of slip angle, θ, for a dimer with intermolecular separation d = 15 Å in (a) and d = 40 Å in (b). The molecular parameters are the same as those in Figure 5. In (a), the ground-state energy correction is smaller and phase II is clearly much narrower as compared to Figure 5; in (b), phase II vanishes entirely. The red hollow circles represent the excited-state energy corrections evaluated under the point dipole approximation (eqs 14a and 14b), whereas the black circles represent the ground-state energy correction under the point quadrupole approximation (eq 14c).

In phase II, defined by slip angles in the range, 26.9° < θ < 38.1°, the bright $|gc\rangle^{AS}$ state continues to lie above the dark state $|gc\rangle^{S}$, unambiguously defining H-aggregates, but the dimer experiences a spectral red shift (vs the monomer) by as much as ∼600 cm^{-1}, leading to the oxymoronic *red-shifted* H-aggregate of Sanyal et al.[26] Finally, in phase III, arrived at when θ < 26.9°, the order of the $|gc\rangle^{AS}$ and $|gc\rangle^{S}$ states reverses so that the bright state is now lower than the dark state, unambiguously defining J-aggregates, whereas the transition energy remains red-shifted relative to the monomer, that is, phase III corresponds to the conventional (Kasha) J-aggregate behavior. In this region, the bright state serves as both the absorption and emission origin and fluorescence is enhanced relative to a monomer, as shown in greater detail in the following section.

Figure 5 also shows selected points of the state energies when the Coulomb coupling in eq 8b is treated exactly. Interestingly, although there are some significant deviations between the first-order corrections and the exact energies mainly within phases I and II—the slip angles which define the phase boundaries are very similar. The most significant deviation occurs for the symmetric state in phase II, attributed to the off-diagonal coupling term between $|gc\rangle^{S}$ and higher-energy symmetric states, which reaches a maximum in phase II.

We can obtain some insights into the origin of phase II by further analyzing the first-order corrections in eqs 12a−12c. The slip angle $\theta_{I,II}$ defining the division between phase I and phase II is determined by setting the dimer absorption peak shift (relative to the monomer) to zero. Using eqs 12a and 12c, we obtain

$$V_{11} + V_{22} - \frac{\rho}{2}(V_{11} + V_{22} + V_{12} + V_{21}) = 0$$

By Taylor expanding the interaction energies in powers of l/d and collecting terms, this becomes

$$\frac{2}{d^3}(1 - 3\cos^2\theta_{I,II}) - \frac{l^2(\rho/2 + 1/6)}{d^5}(9 - 90\cos^2\theta_{I,II} + 105\cos^4\theta_{I,II}) = 0 \quad (13a)$$

where the first and second terms derive from the dipole−dipole and quadrupole−quadrupole interaction energies, respectively. Continuing, the slip angle $\theta_{II,III}$ which divides phase II and phase III is determined by setting the bright and dark state energies equal to each other. Using eqs 12a and 12b, this results in the condition, $V_{11} + V_{22} = V_{12} + V_{21}$, which, upon Taylor expansion, becomes

$$\frac{2}{d^3}(1 - 3\cos^2\theta_{II,III}) - \frac{2l^2}{3d^5}(9 - 90\cos^2\theta_{II,III} + 105\cos^4\theta_{II,III}) = 0 \quad (13b)$$

In the far-field limit ($d \gg l$), the dipole−dipole term dominates and eqs 13a and 13b become identical, giving $\theta_{I,II} = \theta_{II,III}$ = 54.7°, the magic angle at which the point dipole interaction vanishes. Hence, there is no phase II region in the far field and the usual Kasha definitions of H- and J-aggregates follow. However, as the two chromophores approach each other, the O[$1/d^5$] quadrupolar terms become comparable to the O[$1/d^3$] terms. When these terms are included, eqs 13a and 13b are distinct for class I and II chromophores, defined by $0 \le \rho \le 0.5$.[25] Therefore, no single value of θ can satisfy both equations, allowing for the emergence of phase II and the red-shifted H-aggregate. (Interestingly, the equations are identical only when ρ = 1, i.e., for class III dyes in which the ground state $|g\rangle$ is given by $|Z_+\rangle$.[25] The absence of phase II when ρ = 1 is related to the fact that the quadrupole moment is now identical in the ground state, $|g\rangle$, and one-photon allowed excited state, $|c\rangle$).

To further explore the origin of phase II, we show in Figure 6 the dependence of the state energies on the slip angle for much greater intermolecular distances (d = 15 and 40 Å) than that in Figure 5. For these distances, the fully numerically

DOI: 10.1021/acs.jpcc.8b11416
J. Phys. Chem. C 2019, 123, 3203−3215

calculated energies are essentially identical to the first-order corrections and are not plotted. The width of phase II is seen to diminish rapidly with increasing d, practically vanishing, as anticipated, when the two chromophores are sufficiently far apart ($d \gg l$). In this limit, the first-order energy corrections for the two excited states derived from eqs 12a and 12b are dominated by (point) dipole−dipole coupling

$$E^{(1)}_{|gc\rangle^S} = -\frac{\mu_{mon}^{\ 2}}{4\pi\varepsilon_0\varepsilon d^3}(1 - 3\cos^2\theta) \tag{14a}$$

$$E^{(1)}_{|gc\rangle^{AS}} = \frac{\mu_{mon}^{\ 2}}{4\pi\varepsilon_0\varepsilon d^3}(1 - 3\cos^2\theta) \tag{14b}$$

where $\mu_{mon} = el\sqrt{\rho}$ is the monomer TDM. The first-order correction to the ground-state energy is dominated by the (point) quadrupole−quadrupole interaction

$$E^{(1)}_{|gg\rangle} = \frac{Q_{xx}^{\ 2}}{16\pi\varepsilon_0\varepsilon d^5}(9 - 90\cos^2\theta + 105\cos^4\theta) \tag{14c}$$

where $Q_{xx} = \rho el^2$ is the quadrupole moment in the monomer ground state. As can be appreciated from Figure 6b, eqs 14a−14c accurately describe the first-order interaction energies in the limit $d \gg l$.

The dipole−dipole interactions in eqs 14a and 14b were emphasized by Kasha[15−17] in defining J- and H-aggregates. The quadrupole−quadrupole interaction in eq 14c is much shorter in range and can be neglected in comparison to the dipole−dipole terms in eqs 14a and 14b when $d \gg l$. Hence, at sufficiently large intermolecular distances, the ESM and Frenkel exciton model yield identical results for the definition and properties of H- and J-aggregates, in particular, an interconversion at the magic angle, 54.7° It is worth noting here that in the near field, phase I extends beyond the magic angle (see Figure 5). This has further importance because for a random distribution of quadrupoles with a low average intermolecular separation, the blue-shifted H-aggregate spectra will dominate the spectroscopy as well as the electronic energy transfer, which also classically depends on the dipole−dipole interaction. Such a prediction will be tested experimentally in future work.

4.2. HB dimers. For HB packing structures, the optical transitions from the ground state to both excited states are allowed because of the oblique TDM orientation, leading to Davydov splitting. The two excited states can be defined by their symmetries with respect to a C_2 rotation axis as indicated in Figure 4, with the angle between the molecular axis and the C_2 axis defined as ϕ. The TDMs from the ground state to the two excited states are polarized either along the x or y axis (defined in Figure 4)

$$\langle gg|\hat{\mu}|gc\rangle^S = el\sqrt{2\rho}\cos\phi\boldsymbol{j} \tag{15a}$$

$$\langle gg|\hat{\mu}|gc\rangle^{AS} = el\sqrt{2\rho}\sin\phi\boldsymbol{i} \tag{15b}$$

where $\boldsymbol{i}$ and $\boldsymbol{j}$ are unit vectors along the x- and y-axes, respectively. Hence, when $\phi = 0°$, the two molecules are exactly face-to-face and the transition to $|gc\rangle^S$ is allowed only along the y axis; when $\phi = 90°$, the molecules are "head-to-tail" aligned and the transition to $|gc\rangle^{AS}$ is allowed along the x axis. For general values of ϕ, the transitions are allowed along both axes. We expect the y-polarized component to be H-like, whereas we expect the x-polarized component to be J-like.

The first-order energy corrections for the HB dimer are plotted as a function of ϕ in Figure 7, where the distance d is

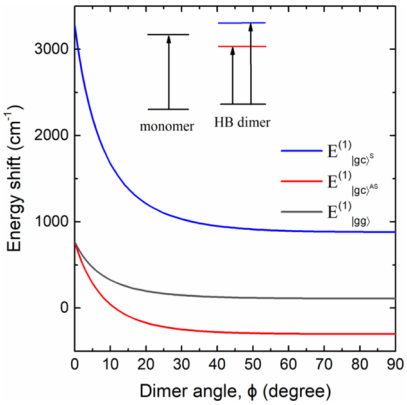

Figure 7. Calculated first-order energetic shifts of the ground state, $|gg\rangle$ (black line), the symmetric excited state, $|gc\rangle^S$ (blue line), and the antisymmetric excited state, $|gc\rangle^{AS}$ (red line) as a function of angle ϕ for an HB dimer (with d = 4 Å). The same molecular parameters are used as in Figure 5. The relative ordering of the electronic states of the dimer versus the monomer is shown in the inset, resulting in the allowed blue- and red-shifted transitions that are respectively y- and x-polarized.

taken to be 4 Å. For the entire range of ϕ values, the symmetric (y-polarized) states lie atop the antisymmetric (x-polarized) state. The energy correction for the ground state lies in between that for the two excited states, such that the resulting Davydov-split peaks straddle the original monomer transition peak. Hence, the upper Davydov component maintains the spectral shift of an H-aggregate, whereas the lower Davydov component maintains the spectral shift of a J-aggregate. As we show below, the vibronic signatures derived from the exciton theory[30,32,33] are also in agreement with H- and J-aggregate behavior for the upper and lower Davydov components. Finally, note that the distance d impacts the magnitude of the energy shifts but does not alter the relative order of the states.

5. SPECTRAL SIGNATURES

In this section, we evaluate the absorption and emission spectra of quadrupolar dimers using the full Hamiltonian, including vibronic coupling, in eq 5 and the expressions for absorption and emission, eqs S12 and S13, respectively. One goal is to determine if the vibronic signatures for H- and J-dimers derived from the exciton theory[30,32,33] remain valid in the ESM. Because of the additional vibrational degrees of freedom, there are a multitude of (dark) symmetric and (bright) antisymmetric states hosting varying numbers of vibrational quanta. Here, we evaluate the eigenstates and energies of the Hamiltonian in eq 5 numerically, after expressing it in an electronic/vibrational basis set which identifies the electronic state of each chromophore, along with the number of vibrational quanta in each nuclear "arm" oscillator (see the Supporting Information for more details). This is accomplished for the quadrupolar SS and HB dimers using the same geometrical parameters as Figures 5 and 7.

The numerically evaluated absorption and PL spectra for a quadrupolar SS dimer as a function of slip angle θ is illustrated in Figure 8. The fluorescence spectra are calculated by assuming that the emission takes place *entirely* from the lowest-energy excited state in accord with Kasha's rule.[44]

DOI: 10.1021/acs.jpcc.8b11416
J. Phys. Chem. C 2019, 123, 3203−3215

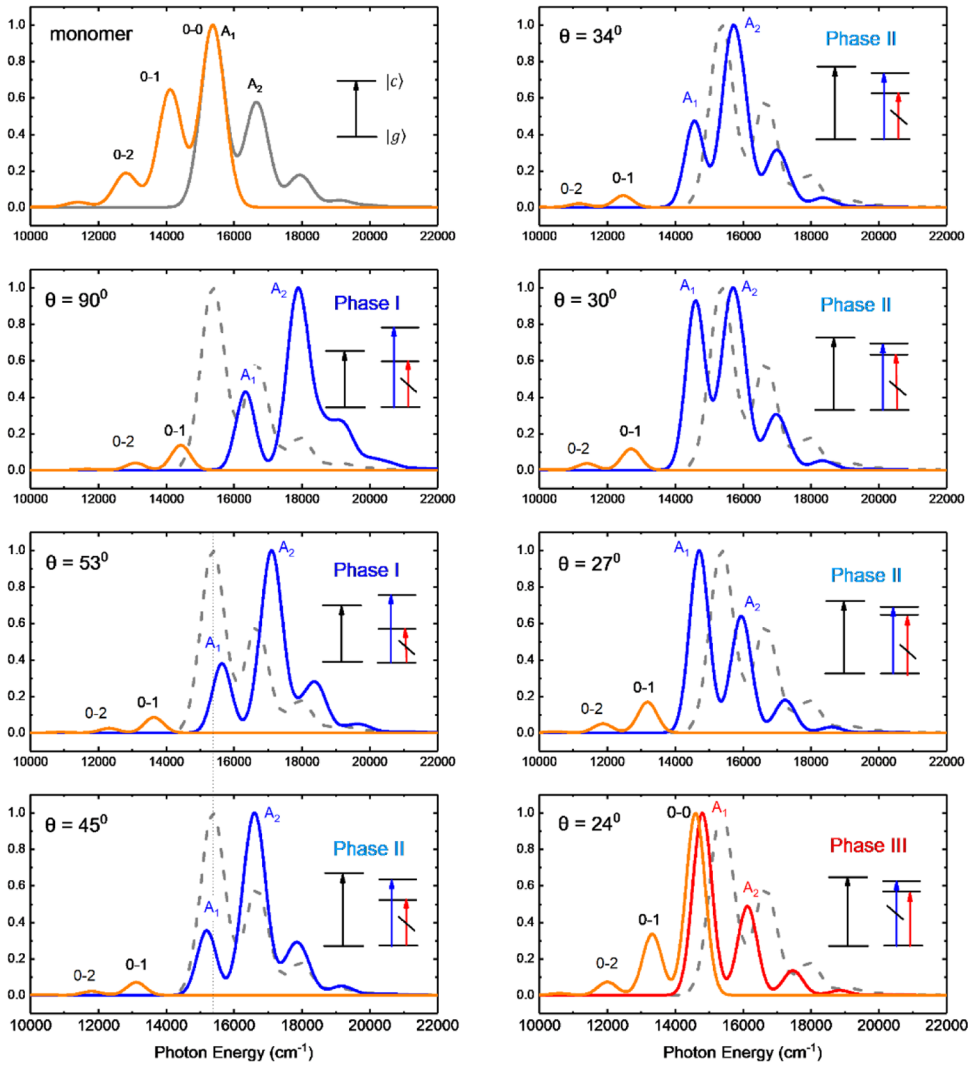

Figure 8. Upper left: Calculated absorption spectrum (gray) and fluorescence spectrum (orange) for a SQ monomer parameterized as in Figure 5 (η = 0.7 eV and t_Z = 1 eV). In addition, the vibrational energy is taken to be $\hbar\omega_{vib}$ = 0.16 eV, characteristic of SQ dyes, but with an enlarged diabatic HR factor (λ_{dia}^2 = 3) to emphasize the vibronic progression. Subsequent panels give the spectra for SS dimers with l and d set to 6 and 4 Å, respectively, as a function of slip angle θ. The absorption spectrum for H-dimers (J-dimers) is shown in blue (red), whereas the fluorescence spectra for either type are shown in orange. (Note that in the lower right panel, the emission spectrum is slightly red-shifted by 200 cm^{-1} for clarity.) The monomer absorption spectrum (gray dashed line) is reproduced in each panel for comparison. The relative ordering of the dimer and monomer energy levels is shown in the inset. All absorption spectra are peak-normalized. The PL spectrum for a given θ is normalized to the peak of the corresponding absorption spectrum. All spectra are calculated using eqs S12 and S13.

Because the energies of electronic ground states with large numbers of vibrational quanta can approach the energies of the electronically excited states, a means to clearly identify the lowest-energy *electronically* excited state is required. To this end, the energy and the "zwitterionic character", σ, of each eigenstate were computed. Here, σ is assigned the value of 1 if both molecules are in the zwitterionic state, a value of 1/2 if just one molecule is in the zwitterionic state, and a value of 0 if both molecules are in the neutral state. For example, evaluating the expectation value of σ for the zero-order states in eqs 10a−10c gives

$$\sigma_{|gg\rangle} = \rho \tag{16a}$$

and

$$\sigma_{|gc\rangle^S} = \sigma_{|gc\rangle^{AS}} = \frac{1+\rho}{2} \tag{16b}$$

Thus, if we arrange all eigenstates from the lowest to the highest energy, the emission state can be found by identifying the first state with $\sigma > 0.5$ because ρ lies in the range $0 < \rho < 0.5$ for typical quadrupolar dyes. It should be clarified that the σ values obtained via numerical simulation using the full vibronic Hamiltonian in eq 5 deviate slightly from the expressions in eqs 16a and 16b, which are based on the zeroth-order electronic-only Hamiltonian (eq 8a). Nevertheless, changes in σ still allow one to unambiguously identify the emitting state (see the Supporting Information for more details).

In Figure 8, the monomer absorption spectrum (top left panel) exhibits a prominent vibronic progression characterized by the effective HR factor, λ^2, evaluated to be approximately 0.6 by substituting λ_{dia}^2 = 3 into eq 7 (see also Figure 2). We chose this value of λ_{dia}^2 in order to obtain a more pronounced vibronic progression for evaluating vibronic signatures. Moreover, we take the line strengths in the PL spectrum to be

DOI: 10.1021/acs.jpcc.8b11416
J. Phys. Chem. C 2019, 123, 3203−3215

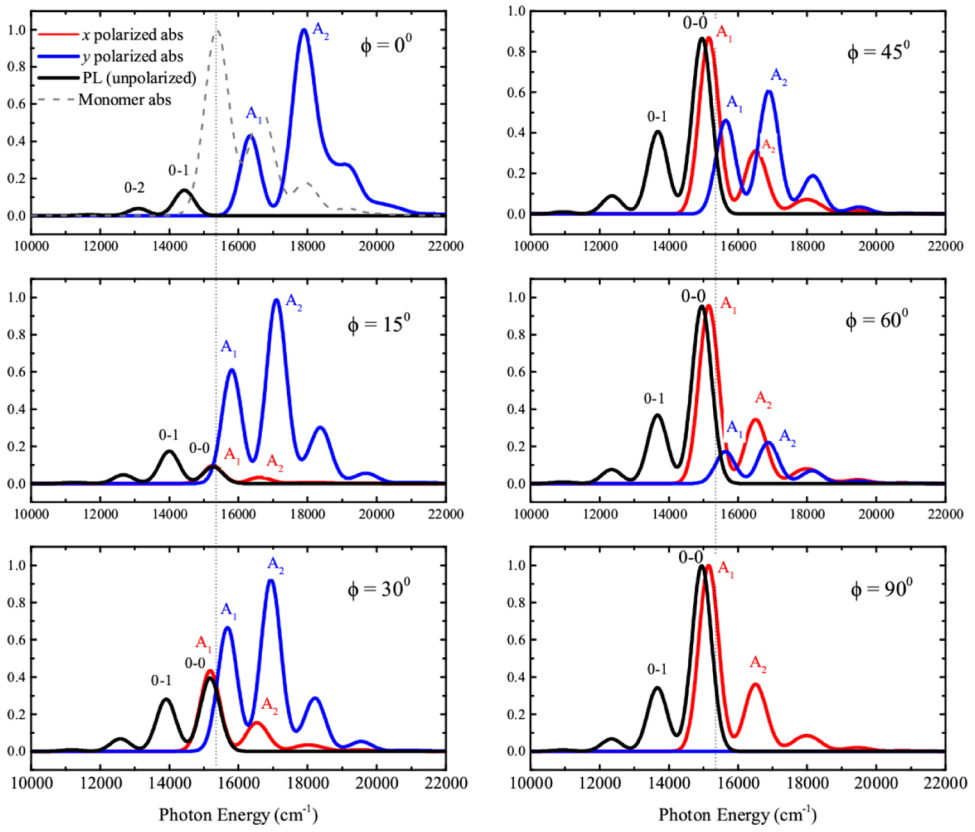

Figure 9. Simulated absorption spectra polarized along the x axis (red curve) and y axis (blue curve) of an HB dimer as a function of ϕ. The PL spectrum shown in black represents the sum of the x- and y-components for clarity. The peak in the monomer absorption is indicated by the gray line throughout for comparison. Molecular parameters are the same as in Figure 8. For the right panels, the PL spectrum is slightly red-shifted (by 200 cm^{-1}) for clarity.

governed entirely by the oscillator strength,[45] as in the absorption spectrum (see eqs S12 and S13), to make the two spectra easier to compare. As shown in the figure, the fluorescence spectrum is very close to the "mirror image" of the absorption spectrum. On the basis of the ratio of the first two vibronic peaks in the fluorescence spectrum (see eq 6), the HR factor is ≈0.65, close to the value of $\lambda^2 \approx 0.60$ determined from the absorption spectrum. The slight discrepancy is likely a result of the approximations inherent in the perturbative treatment required to justify an effective HR factor in the ESM.

The dimer spectra in Figure 8 are displayed for several slip angles, θ, starting with the eclipsed ("side-by-side") geometry with $\theta = 90°$. For slip angles in the range, $90° < \theta < 53°$, the absorption bands are significantly blue-shifted—by as much as ∼1000 cm^{-1} based on the first vibronic peak (A_1)—with a concomitant suppression of the fluorescence emission, entirely consistent with the phase-I H-dimer predicted in Figure 5. Moreover, the vibronic signatures are entirely consistent with those predicted from the vibronic exciton theory:[30,32,33] the 0−0 PL band vanishes completely because the lowest-energy (emitting) state is dark, and the A_1/A_2 ratio of oscillator strengths in the absorption spectrum is suppressed compared to the monomer value.

A slip angle of 45° marks the entry into the unconventional phase II region. Note that this value of the slip angle is slightly larger than the value of 38.1° in Figure 5 because of the inclusion of vibronic coupling terms in Figure 8. In phase II, the dimer vibronic peaks are now *red-shifted* compared to the corresponding peaks in the monomer band (note in particular the red shift of the A_1 peak). Moreover, the fluorescence remains suppressed as in phase I, the 0−0 PL peak remains absent because of the dark emitting state, and the A_1/A_2 absorption spectral ratio remains smaller than the monomer. In other words, the red-shifted H-aggregate of phase II abides by all the *vibronic* signatures, which identify H-aggregates from the exciton theory.

When $\theta < 24.7°$—close to the value of 26.9° predicted from Figure 5—the aggregate enters phase III. As shown in Figure 8, the absorption peaks remain red-shifted relative to the monomer, but the aggregate becomes strongly emissive, as is characteristic of a conventional J-aggregate. Note especially the rise and dominance of the 0−0 PL component. This behavior is a result of the bright state moving below the dark state(s) as θ slips below 24.7°, thereby providing both strong absorption and pronounced 0−0 emission. In phase III, the ratio A_1/A_2 exceeds that of the monomer, in contrast to what was found for the red-shifted H-aggregate in phase II, and consistent with the vibronic signatures of J-aggregates derived from the vibronic exciton theory.[30,32,33] Moreover, the 0−0/0−1 peak intensity ratio of approximately three in the PL spectrum is closely approximated by the vibronic exciton expression[33]

$$I_{PL}^{0-0}/I_{PL}^{0-1} = N/\lambda^2$$

where $N = 2$ for the dimer and $\lambda^2 = 0.65$ is the effective monomer HR factor evaluated from the PL spectrum in Figure 8. (In this expression, $I_{PL}^{0-\nu}$ is strictly defined as the line strength solely because of the square of the TDM.) Hence, all of the vibronic features evident in phase III are fully consistent

DOI: 10.1021/acs.jpcc.8b11416
J. Phys. Chem. C 2019, 123, 3203−3215

with the vibronic signatures of J-aggregation derived from the vibronic exciton theory. Although not shown, we have verified numerically that for much larger intermolecular distances, the magic angle of 54.7° is the point at which the phase I/phase III conversion takes place (phase II vanishes, see Figure 6b) even when vibronic coupling is present.

We should point out, however, some peculiar spectral features which distinguish the ESM from the Frenkel exciton model. For example, as θ increases beyond 34°, the A_1/A_2 vibronic peak ratio remains remarkably stable (and less than the monomer value as is consistent with H-aggregation) and hardly changes despite a steady blue shift of the vibronic peaks. However, as θ *decreases* below 34°, the absorption band shifts remain stable, but the redistribution of the vibronic peak intensity is dramatic. Furthermore, there are small discrepancies between the peak ratio and the excited state ordering. Specifically, in the small interval near the boundary between phase II and III with θ in the range 24.7°−26.3°, the A_1/A_2 ratio is larger than that of the monomer (J-like), but the bottom of the excited state band is still a dark state, indicating an H-aggregate; a J-aggregate with the characteristic prominent 0−0 fluorescence peak can be clearly identified only when θ drops below 24.7°.

Finally, we also simulated the absorption and emission spectra for the HB dimer, as shown in Figure 9. The absorption spectrum is divided into components polarized in the x and y directions defined in Figure 4, corresponding to transitions to the antisymmetric and symmetric states (defined wrt. the twofold rotation), respectively. Figure 9 shows that the spectra evolve from pure H-like at $\phi = 0$ to pure J-like at $\phi = 90$ as expected from the dimer geometries in Figure 4 and consistent with the results of Sanyal et al.[26] Note that the y-polarized component is H-like throughout; the spectrum is blue-shifted relative to the monomer and the A_1/A_2 ratio is smaller than the monomer value. Conversely, the x-polarized component is J-like throughout: the spectrum is red-shifted and the A_1/A_2 ratio is larger than the monomer value. Hence, the H- and J-behaviors coincide closely with those predicted from the vibronic exciton model.[30,32,33] This remains true for the PL spectrum as well; the 0−0 peak is entirely absent in the ideal H-aggregate with $\phi = 0$ and steadily grows in as the HB angle increases, becoming maximum in the J-configuration when $\phi = 90$. Although not indicated in the figure, the 0−0 component is exclusively x-polarized, as it arises from the low-energy J-like (antisymmetric) emitting state (see Figure S4).

6. CONCLUSIONS

In this work, we applied the ESM enhanced to include vibronic coupling to monomers and dimer aggregates of DAD quadrupolar dye molecules. We exploited the vibronic structure in the absorption and emission spectra to establish important connections between the ESM and Frenkel exciton models. Already at the monomer level, the differences are profound; the ESM predicts that the vibronic progression, as governed by an adiabatic HR factor (see eq 7), is sensitive to the mixing of neutral and charge-transfer diabatic states to create the (adiabatic) ground and excited states.[25] The mixing is also sensitive to intermolecular interactions within an aggregate; it is therefore not that surprising that under certain circumstances, the spectral properties of quadrupolar aggregates can diverge significantly from the conventional H- and J-aggregate behavior predicted using Kasha's exciton model. In particular, in the "red-shifted H-aggregate" introduced by Sanyal et al.,[26] the bright state remains higher in energy than the dark state (as unambiguously defines H-aggregates), although the bright state transition energy lies *below* the monomer transition energy. As shown here, this unusual aggregate type is created by strong quadrupole−quadrupole interactions and persists in the presence of vibronic coupling. It exists over a range of intermolecular slip angles defining what we refer to as phase II, which divides conventional H-aggregate behavior (phase I) and J-aggregate (phase III) behavior. Phase II arises when the quadrupole−quadrupole interaction, which scales as $O[1/R^5]$, becomes comparable to the dipole−dipole interaction, which scales as $O[1/R^3]$. Phase II therefore vanishes in the far-field limit ($d \gg l$), where only conventional Kasha H- and J-aggregates are possible, with the interconversion occurring at the magic angle (see Figure 6b).

Quite remarkably, the red-shifted H-aggregate still abides by all of the vibronic signatures characterizing H-aggregates derived from the vibronic Frenkel exciton theory;[30,32,33] the A_1/A_2 ratio in the absorption spectrum is attenuated compared to the monomer and the 0−0 peak in the PL spectrum is entirely absent. Moreover, in the conventional H- and J-aggregate regions (phase I and III, respectively), the vibronic signatures match what is expected for J- and H-aggregates using the vibronic Frenkel exciton model.

We further analyzed HB-type dimers where the oscillator strength is generally distributed among both symmetric and antisymmetric excited states, leading to Davydov splitting[26,34−36] in the absorption spectrum, in agreement with Sanyal et al.[26] Again, the vibronic signatures expressed in the blue-shifted H-like polarization component and the red-shifted J-like polarization component abide by the signatures derived from the vibronic exciton theory.[30,32,33] Notably, the A_1/A_2 ratio exceeds the monomer value in the J-like component but is smaller than the monomer value in the H-like component.

We should point out, however, that the aforementioned close agreement between the vibronic exciton theory and the ESM with respect to spectral signatures is based largely on a first-order treatment of the Coulombic coupling energy within a dimer. Much stronger couplings resulting from unscreened potentials and smaller intermolecular contact distances may result in the formation of low-energy biexcitons and even exciton strings in which the ground state resembles a charge density wave. Such unusual entities have been discussed theoretically by Painelli and coworkers[26,46] but have not, to our knowledge, been unambiguously observed in real systems.

In future work, we will establish whether the vibronic spectral signatures under the ESM remain reliable indicators of J- and H-aggregation for DA complexes, as exemplified by the merocyanine class of dyes. Merocyanine dyes have recently been shown to aggregate with classic Kasha-like H- and J-aggregate line shapes.[47] We also wish to explore the strong coupling regime in order to determine whether there are vibronic spectral signatures indicating the formation of biexcitons and exciton "strings".[26,46] It would also be worthwhile to investigate possible interferences between intermolecular charge transfer[41,48,49] and Coulombic coupling. Such interferences are known to impact the photophysical response in Frenkel/CT exciton complexes.[30,31,50] Finally, a more detailed analysis of the impact of short-range Coulombic interactions on the energy-transfer rates is warranted to better understand the extent to which quadrupole−quadrupole interactions in quadrupolar dyes may influence optoelectronic device performance.

DOI: 10.1021/acs.jpcc.8b11416
J. Phys. Chem. C 2019, 123, 3203−3215

■ ASSOCIATED CONTENT

Supporting Information

The Supporting Information is available free of charge on the ACS Publications website at DOI: 10.1021/acs.jpcc.8b11416.

Product basis set for vibronic excitations, derivation of the HR factor for quadrupolar monomers, and evaluation of the dimer energies and optical spectra (PDF)

■ AUTHOR INFORMATION

Corresponding Author

*E-mail: spano@temple.edu.

ORCID

Frank C. Spano: 0000-0003-3044-6727

Notes

The authors declare no competing financial interest.

■ ACKNOWLEDGMENTS

This work was carried out with the financial support for C.Z. and C.J. from the National Science Foundation (CBET-1603372) and for C.Z. and F.C. from the National Science Foundations (SusChEM-1603461).

■ REFERENCES

(1) Gsänger, M.; Bialas, D.; Huang, L.; Stolte, M.; Würthner, F. Organic Semiconductors based on Dyes and Color Pigments. *Adv. Mater.* **2016**, *28*, 3615−3645.

(2) Wang, B.; Wang, Y.; Hua, J.; Jiang, Y.; Huang, J.; Qian, S.; Tian, H. Starburst Triarylamine Donor-Acceptor-Donor Quadrupolar Derivatives Based on Cyano-Substituted Diphenylaminestyrylbenzene: Tunable Aggregation-Induced Emission Colors and Large Two-Photon Absorption Cross Sections. *Chem.—Eur. J.* **2011**, *17*, 2647−2655.

(3) Zheng, C.; Jalan, I.; Cost, P.; Oliver, K.; Gupta, A.; Misture, S.; Cody, J. A.; Collison, C. J. Impact of Alkyl Chain Length on Small Molecule Crystallization and Nanomorphology in Squaraine-Based Solution Processed Solar Cells. *J. Phys. Chem. C* **2017**, *121*, 7750−7760.

(4) Zheng, C.; Bleier, D.; Jalan, I.; Pristash, S.; Penmetcha, A. R.; Hestand, N. J.; Spano, F. C.; Pierce, M. S.; Cody, J. A.; Collison, C. J. Phase separation, crystallinity and monomer-aggregate population control in solution processed small molecule solar cells. *Sol. Energy Mater. Sol. Cells* **2016**, *157*, 366−376.

(5) Chen, G.; Sasabe, H.; Igarashi, T.; Hong, Z.; Kido, J. Squaraine dyes for organic photovoltaic cells. *J. Mater. Chem. A* **2015**, *3*, 14517−14534.

(6) Yang, D.; Sasabe, H.; Jiao, Y.; Zhuang, T.; Huang, Y.; Pu, X.; Sano, T.; Lu, Z.; Kido, J. An effective π-extended squaraine for solution-processed organic solar cells with high efficiency. *J. Mater. Chem. A* **2016**, *4*, 18931−18941.

(7) Goh, T.; Huang, J.-S.; Yager, K. G.; Sfeir, M. Y.; Nam, C.-Y.; Tong, X.; Guard, L. M.; Melvin, P. R.; Antonio, F.; Bartolome, B. G.; Lee, M. L.; Hazari, N.; Taylor, A. D. Quaternary Organic Solar Cells Enhanced by Cocrystalline Squaraines with Power Conversion Efficiencies > 10%. *Adv. Energy Mater.* **2016**, *6*, 1600660.

(8) Ahn, H.-Y.; Yao, S.; Wang, X.; Belfield, K. D. Near-Infrared-Emitting Squaraine Dyes with High 2PA Cross-Sections for Multiphoton Fluorescence Imaging. *ACS Appl. Mater. Interfaces* **2012**, *4*, 2847−2854.

(9) Yuan, L.; Lin, W.; Zheng, K.; He, L.; Huang, W. Far-red to near infrared analyte-responsive fluorescent probes based on organic fluorophore platforms for fluorescence imaging. *Chem. Soc. Rev.* **2013**, *42*, 622−661.

(10) Beverina, L.; Salice, P. Squaraine Compounds: Tailored Design and Synthesis towards a Variety of Material Science Applications. *Eur. J. Org. Chem.* **2010**, *2010*, 1207−1225.

(11) Liu, X.; Sun, Y.; Hsu, B. B. Y.; Lorbach, A.; Qi, L.; Heeger, A. J.; Bazan, G. C. Design and Properties of Intermediate-Sized Narrow Band-Gap Conjugated Molecules Relevant to Solution-Processed Organic Solar Cells. *J. Am. Chem. Soc.* **2014**, *136*, 5697−5708.

(12) Carlé, J. E.; Krebs, F. C. Technological status of organic photovoltaics (OPV). *Sol. Energy Mater. Sol. Cells* **2013**, *119*, 309−310.

(13) Bergemann, K. J.; Forrest, S. R. Measurement of exciton diffusion lengths in optically thin organic films. *Appl. Phys. Lett.* **2011**, *99*, 243303.

(14) Wei, G.; Lunt, R. R.; Sun, K.; Wang, S.; Thompson, M. E.; Forrest, S. R. Efficient, Ordered Bulk Heterojunction Nanocrystalline Solar Cells by Annealing of Ultrathin Squaraine Thin Films. *Nano Lett.* **2010**, *10*, 3555−3559.

(15) McRae, E. G.; Kasha, M. Enhancement of phosphorescence ability upon aggregation of dye molecules. *J. Chem. Phys.* **1958**, *28*, 721−722.

(16) Kasha, M.; Rawls, H. R.; El-Bayoumi, M. A. *The Exciton Model in Molecular Spectroscopy*; Butterworths: London, 1965; Vol. *11*.

(17) Kasha, M. Energy Transfer Mechanisms and the Molecular Exciton Model for Molecular Aggregates. *Radiat. Res.* **1963**, *20*, 55−70.

(18) Scheibe, G. *Optische Anregungen Organischer Systeme*; Forst, W., Ed.; Verlag Chemie: Weinheim, 1966; p 109.

(19) Möbius, D. Scheibe Aggregates. *Adv. Mater.* **1995**, *7*, 437−444.

(20) Daltrozzo, E.; Scheibe, G.; Gschwind, K.; Haimerl, F. Structure of J-Aggregates of Pseudoisocyanine. *Photogr. Sci. Eng.* **1974**, *18*, 441−450.

(21) Würthner, F.; Saha-Möller, C. R.; Fimmel, B.; Ogi, S.; Leowanawat, P.; Schmidt, D. Perylene Bisimide Dye Assemblies as Archetype Functional Supramolecular Materials. *Chem. Rev.* **2016**, *116*, 962−1052.

(22) Philpott, M. R. Dipole Davydov Splittings in Crystalline Anthracene, Tetracene, Naphthalene, and Phenanthrene. *J. Chem. Phys.* **1969**, *50*, 5117−5128.

(23) Shafeekh, K. M.; Das, S.; Sissa, C.; Painelli, A. Asymmetric Squaraine Dyes: Spectroscopic and Theoretical Investigation. *J. Phys. Chem. B* **2013**, *117*, 8536−8546.

(24) Grisanti, L.; D'Avino, G.; Painelli, A.; Guasch, J.; Ratera, I.; Veciana, J. Essential State Models for Solvatochromism in Donor−Acceptor Molecules: The Role of the Bridge. *J. Phys. Chem. B* **2009**, *113*, 4718−4725.

(25) Terenziani, F.; Painelli, A.; Katan, C.; Charlot, M.; Blanchard-Desce, M. Charge instability in quadrupolar chromophores: Symmetry breaking and solvatochromism. *J. Am. Chem. Soc.* **2006**, *128*, 15742−15755.

(26) Sanyal, S.; Painelli, A.; Pati, S. K.; Terenziani, F.; Sissa, C. Aggregates of quadrupolar dyes for two-photon absorption: the role of intermolecular interactions. *Phys. Chem. Chem. Phys.* **2016**, *18*, 28198−28208.

(27) Zhang, Y.; Kim, B.; Yao, S.; Bondar, M. V.; Belfield, K. D. Controlled Aggregation and Enhanced Two-Photon Absorption of a Water-Soluble Squaraine Dye with a Poly(acrylic acid) Template. *Langmuir* **2013**, *29*, 11005−11012.

(28) Spano, F. C. Analysis of the UV/Vis and CD Spectral Line Shapes of Carotenoid Assemblies: Spectral Signatures of ChiralH-Aggregates. *J. Am. Chem. Soc.* **2009**, *131*, 4267−4278.

(29) Clark, J.; Silva, C.; Friend, R. H.; Spano, F. C. Role of intermolecular coupling in the photophysics of disordered organic semiconductors: Aggregate emission in regioregular polythiophene. *Phys. Rev. Lett.* **2007**, *98*, 206406.

(30) Hestand, N. J.; Spano, F. C. Expanded Theory of H- and J-Molecular Aggregates: The Effects of Vibronic Coupling and Intermolecular Charge Transfer. *Chem. Rev.* **2018**, *118*, 7069−7163.

DOI: 10.1021/acs.jpcc.8b11416
J. Phys. Chem. C 2019, 123, 3203−3215

(31) Hestand, N. J.; Spano, F. C. Molecular Aggregate Photophysics beyond the Kasha Model: Novel Design Principles for Organic Materials. *Acc. Chem. Res.* **2017**, *50*, 341−350.
(32) Spano, F. C. The Spectral Signatures of Frenkel Polarons in H- and J-Aggregates. *Acc. Chem. Res.* **2010**, *43*, 429−439.
(33) Spano, F. C.; Yamagata, H. Vibronic Coupling in J-Aggregates and Beyond: A Direct Means of Determining the Exciton Coherence Length from the Photoluminescence Spectrum. *J. Phys. Chem. B* **2011**, *115*, 5133−5143.
(34) Röhr, M. I. S.; Marciniak, H.; Hoche, J.; Schreck, M. H.; Ceymann, H.; Mitric, R.; Lambert, C. Exciton Dynamics from Strong to Weak Coupling Limit Illustrated on a Series of Squaraine Dimers. *J. Phys. Chem. C* **2018**, *122*, 8082−8093.
(35) Lambert, C.; Koch, F.; Völker, S. F.; Schmiedel, A.; Holzapfel, M.; Humeniuk, A.; Röhr, M. I. S.; Mitric, R.; Brixner, T. Energy Transfer Between Squaraine Polymer Sections: From Helix to Zigzag and All the Way Back. *J. Am. Chem. Soc.* **2015**, *137*, 7851−7861.
(36) Balzer, F.; Kollmann, H.; Schulz, M.; Schnakenburg, G.; Lützen, A.; Schmidtmann, M.; Lienau, C.; Silies, M.; Schiek, M. Spotlight on Excitonic Coupling in Polymorphic and Textured Anilino Squaraine Thin Films. *Cryst. Growth Des.* **2017**, *17*, 6455−6466.
(37) Brixner, T.; Hildner, R.; Köhler, J.; Lambert, C.; Würthner, F. Exciton Transport in Molecular Aggregates - From Natural Antennas to Synthetic Chromophore Systems. *Adv. Energy Mater.* **2017**, *7*, 1700236.
(38) Law, K.-Y. Squaraine Chemistry. Absorption, Fluorescence Emission, and Photophysics of Unsymmetrical Squaraines. *J. Phys. Chem.* **1995**, *99*, 9818−9824.
(39) Zheng, C.; Penmetcha, A. R.; Cona, B.; Spencer, S. D.; Zhu, B.; Heaphy, P.; Cody, J. A.; Collison, C. J. Contribution of Aggregate States and Energetic Disorder to a Squaraine System Targeted for Organic Photovoltaic Devices. *Langmuir* **2015**, *31*, 7717−7726.
(40) Liu, T.; Liu, X.; Wang, W.; Luo, Z.; Liu, M.; Zou, S.; Sissa, C.; Painelli, A.; Zhang, Y.; Vengris, M.; Bondar, M. V.; Hagan, D. J.; Van Stryland, E. W.; Fang, Y.; Belfield, K. D. Systematic Molecular Engineering of a Series of Aniline-Based Squaraine Dyes and Their Structure-Related Properties. *J. Phys. Chem. C* **2018**, *122*, 3994−4008.
(41) Hestand, N. J.; Zheng, C.; Penmetcha, A. R.; Cona, B.; Cody, J. A.; Spano, F. C.; Collison, C. J. Confirmation of the Origins of Panchromatic Spectra in Squaraine Thin Films Targeted for Organic Photovoltaic Devices. *J. Phys. Chem. C* **2015**, *119*, 18964−18974.
(42) Kurhuzenkau, S. A.; Colon Gomez, M. Y.; Belfield, K. D.; Shaydyuk, Y. O.; Hagan, D. J.; Van Stryland, E. W.; Sissa, C.; Bondar, M. V.; Painelli, A. Electronic Nature of Nonlinear Optical Properties of a Symmetrical Two-Photon Absorbing Fluorene Derivative: Experimental Study and Theoretical Modeling. *J. Phys. Chem. C* **2018**, *122*, 5664−5672.
(43) Shuai, Z.; Brédas, J. L.; Su, W. P. Nature of photoexcitations in poly (paraphenylene vinylene) and its oligomers. *Chem. Phys. Lett.* **1994**, *228*, 301−306.
(44) Kasha, M. Characterization of Electronic Transitions in Complex Molecules. *Discuss. Faraday Soc.* **1950**, *9*, 14−19.
(45) We are therefore replacing the usual cubic dependence on photon energy in the PL transition intensities with a linear dependence derived from the oscillator strength.
(46) D'Avino, G.; Terenziani, F.; Painelli, A. Aggregates of quadrupolar dyes: Giant two-photon absorption from biexciton states. *J. Phys. Chem. B* **2006**, *110*, 25590−25592.
(47) Liess, A.; Lv, A.; Arjona-Esteban, A.; Bialas, D.; Krause, A.-M.; Stepanenko, V.; Stolte, M.; Würthner, F. Exciton Coupling of Merocyanine Dyes from H- to J-type in the Solid State by Crystal Engineering. *Nano Lett.* **2017**, *17*, 1719−1726.
(48) Guasch, J.; Grisanti, L.; Souto, M.; Lloveras, V.; Vidal-Gancedo, J.; Ratera, I.; Painelli, A.; Rovira, C.; Veciana, J. Intra- and Intermolecular Charge Transfer in Aggregates of Tetrathiafulvalene-Triphenylmethyl Radical Derivatives in Solution. *J. Am. Chem. Soc.* **2013**, *135*, 6958−6967.
(49) Uranga-Barandiaran, O.; Catherin, M.; Zaborova, E.; D'Aléo, A.; Fages, F.; Castet, F.; Casanova, D. Optical properties of quadrupolar and bi-quadrupolar dyes: intra and inter chromophoric interactions. *Phys. Chem. Chem. Phys.* **2018**, *20*, 24623−24632.
(50) Hestand, N. J.; Spano, F. C. Interference between Coulombic and CT-mediated couplings in molecular aggregates: H- to J-aggregate transformation in perylene-based π-stacks. *J. Chem. Phys.* **2015**, *143*, 244707.

DOI: 10.1021/acs.jpcc.8b11416
J. Phys. Chem. C 2019, 123, 3203−3215